Jahn–Teller and off-center defects in $BaTiO_3$: Ni^+, Rh^{2+}, Pt^{3+} and Fe^{5+} as studied by EPR under uniaxial stress

2007 J. Phys.: Condens. Matter 19 496214

(http://iopscience.iop.org/0953-8984/19/49/496214)

IOP PUBLISHING JOURNAL OF PHYSICS: CONDENSED MATTER

J. Phys.: Condens. Matter **19** (2007) 496214 (15pp) doi:10.1088/0953-8984/19/49/496214

Jahn–Teller and off-center defects in $BaTiO_3$: Ni^+, Rh^{2+}, Pt^{3+} and Fe^{5+} as studied by EPR under uniaxial stress

Th W Kool[1], S Lenjer[2] and O F Schirmer[2]

[1] Van 't Hoff Institute for Molecular Sciences, University of Amsterdam, NL 1018 WV Amsterdam, Netherlands
[2] Fachbereich Physik, University of Osnabrück, D-49069 Osnabrück, Germany

Received 12 July 2007, in final form 2 October 2007
Published 15 November 2007
Online at stacks.iop.org/JPhysCM/19/496214

Abstract

Application of uniaxial stress reveals the Jahn–Teller (JT) properties of the defect ions Ni^+ ($3d^9$), Rh^{2+} ($4d^7$) and Pt^{3+} ($5d^7$), all incorporated on Ti^{4+} sites in $BaTiO_3$. In all cases the vibronic ground states are stabilized by an E $\otimes$ e Jahn–Teller effect, here leading to tetragonally elongated defect–O_6 octahedra. Orbitals of $(x^2 - y^2)$ type are thus lowest for the hole-like Ni^+, and $(3z^2 - r^2)$ for the electron-like strong-field cases Rh^{2+} and Pt^{3+}. The three systems are characterized by motionally averaged isotropic spectra at elevated temperatures. At low temperatures strong dependences on the distribution of internal strains are found, leading to a coexistence of isotropic averaged and quasi-static tetragonal situations for Ni^+, becoming more static under uniaxial external stress. The latter behavior is also identified for Rh^{2+}. For Rh^{2+} and Pt^{3+} the coupling of the JT systems to the external stress could be determined quantitatively, predicting rather low JT energies by a simple model calculation. The observation of tetragonal distortions of these defects thus points to the presence of regions with strong internal strains. The impurity ion Fe^{5+} ($3d^3$), also replacing Ti^{4+}, is found to go spontaneously off-center along [111] type directions. The defect axis orients parallel to the stress direction, indicating an axially compressed Fe^{5+}–O_6 oxygen arrangement in the off-center situation.

1. Introduction

$BaTiO_3$ (BT) is a representative member of the large class of oxide perovskites, ABO_3. Its use in many fields of application is supported by the possibility to tailor its properties by incorporating selected defects. Their identity, including their ionic and electronic structure, their energy levels and often also their optical absorptions, could be ascertained in many cases (see, e.g. [1]), mainly by using electron paramagnetic resonance (EPR) and related techniques. The present state of knowledge on defects in BT thus constitutes a basis for the assessment

of their role in other oxide perovskites, where the knowledge about defects is often more scarce. The point defects identified in BT comprise transition metal (see, e.g. [2]) and rare earth ions (see, e.g. [3]). Likewise, intrinsic defects such as free electron Jahn–Teller (JT) polarons and bipolarons [4, 5] as well as hole polarons bound to acceptors have been studied [6]. The microscopic structure of the isolated oxygen vacancy is still under discussion [7].

In the present contribution we add to the knowledge on defects in BT by determining the properties of several transition metal dopings characterized by their JT and off-center instabilities. Because of the underlying coupling to the lattice they show strong responses to the application of external uniaxial stress. This is instrumental for unraveling the details of their interaction with the lattice.

As indicated, the ions Ni^{+}, Rh^{2+}, Pt^{3+} and Fe^{5+} are studied, all incorporated on Ti^{4+} sites. Ni^{+} ($3d^9$) has one hole in the 3d shell. In a sixfold cubic oxygen environment the orbital E doublet lies lowest for holes. An elongation of the octahedron stabilizes the $(x^2 - y^2)$ partner of the doublet. The application of stress will show this case to hold, induced by an E $\otimes$ e JT effect.

When Rh^{2+} ($4d^7$) and Pt^{3+} ($5d^7$) are incorporated into BT, a strong cubic crystal field splitting occurs, and thus the first six electrons are diamagnetically paired in the $(t_2)^6$ subshell. The last electron, $(e)^1$, therefore gives an overall E character to the ions. Here it is found that the $(3z^2 - r^2)$ orbital is the ground state. This also points to an elongation of the surrounding octahedron, stabilizing an electron in such an orbital. All JT cases studied are characterized by a spin $S = 1/2$.

Fe^{5+} ($3d^3$, $S = 3/2$) is isoelectronic to Mn^{4+} and Cr^{3+}, but is likely to have a smaller ionic radius. It thus tends to go strongly off-center along a [111] type direction ($\langle 111 \rangle$) from its Ti^{4+} home site in BT. It will be shown that this is borne out by the trigonal crystal field splittings in the sequence of isoelectronic ions Cr^{3+}, Mn^{4+}, and Fe^{5+}; the latter ion is characterized by an especially strong axial crystal field, separating the $S = 3/2$, $|m_S| = |1/2\rangle$ substates from $|m_S| = |3/2\rangle$ by a considerable energy.

2. Theoretical background of the $E \otimes e$ JT effect

The investigation of this JT situation has a long history (see e.g. [8–16]). We shall list here only those aspects of the relevant theory which are necessary to explain the present results. In cubic symmetry the two orbital partners of an E state are degenerate. A JT distortion along one of the two modes of an e vibration will lift this degeneracy. Assume that a charge carrier, electron or hole, is accommodated in one of the E orbitals, e.g. in φ_z, which has become the ground state by a corresponding JT distortion. Its probability density is tetragonally symmetric around a z-axis, i.e. along the double arrows in figure 1. This situation, stabilized by the corresponding lattice distortion (figure 1), is the result of a static JT effect.

Locally, the lattice vibrates with the amplitudes of the corresponding e-distortion mode, as symbolized in figure 1. Together with the related vibrational function, χ_z, the vibronic eigenstates of the systems are given by the product $\Psi_z = \varphi_z \chi_z$. In an ideal unstrained lattice, all the vibronic states with equivalently oriented axes, $\Psi_x = \varphi_x \chi_x$ and $\Psi_y = \varphi_y \chi_y$, are equally likely to occur as ground states.

In EPR, a nd^9 hole in an elongated octahedron, as in figure 1 (left), having an $(x^2 - y^2)$ ground state, is characterized [10, 11] by an axial g-tensor with the components

$$g_\parallel = g_s - 8k\lambda/\Delta \qquad \text{and} \qquad g_\perp = g_s - 2k\lambda/\Delta. \tag{1}$$

This can alternatively be formulated using the scalar and the tensorial parts, respectively, of the

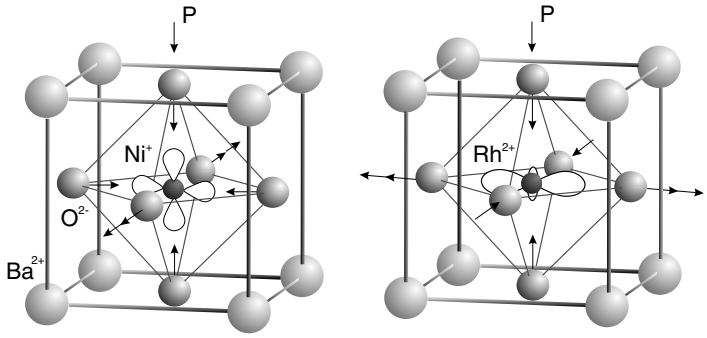

Figure 1. Two types of possible E orbitals, present as ground states in Ni^{+} ($3d^9$), $x^2 - y^2$ type (left), and in Rh^{2+} ($4d^7$) and Pt^{3+} ($5d^7$), $3z^2 - r^2$ type (right). They are shown to be stabilized by the tetragonal partner of an e-vibration mode. P denotes the direction of the axis of the applied stress, which tends to orient the elongated tetragonal distortions with their axes in the plane perpendicular to P, as indicated.

Zeeman interaction, proportional to g_1 and g_2, respectively, by

$$g_{\parallel} = g_1 + 2g_2 \qquad \text{and} \qquad g_{\perp} = g_1 - g_2. \tag{2}$$

Here $g_1 = g_s - 4k\lambda/\Delta$ and $g_2 = -2k\lambda/\Delta$. The spin–orbit coupling of the ion is proportional to the constant λ; it is negative for a hole; k is an orbital reduction factor, and Δ can be approximated by the crystal field splitting of the system in the cubic, undistorted precursor state. For an nd^7 ion in a strong crystal field the admixture of crystal field excited states to the ground state leads to more complicated expressions for the g-tensor [17, 18], because there are several excited crystal field states which can be coupled to the ground state by spin–orbit coupling. It may suffice to state that, in contrast to the d^9 hole case, $g_{\parallel} < g_{\perp}$ is predicted for an electron in a $(3z^2 - r^2)$ state.

If the energy barrier between the equivalent orbital orientations is small enough, the ground state of the system will tunnel between these wells and the corresponding vibronic states, applicable for unimpeded tunneling, will be [10, 11]

$$\Psi(\mathrm{A}) = N_{\mathrm{A}}[\Psi_x + \Psi_y + \Psi_z] \tag{3a}$$

$$\Psi_{\varepsilon}(\mathrm{E}) = N_{\varepsilon}[\Psi_x - \Psi_y] \tag{3b}$$

$$\Psi_{\theta}(\mathrm{E}) = N_{\theta}[2\Psi_z - \Psi_x - \Psi_y], \tag{3c}$$

where the N_i are the relevant normalization constants. The A singlet state lies higher by the tunneling splitting 3Γ than the E vibronic ground states.

Both the static and the tunneling situations of an E $\otimes$ e JT system are borderline cases. Starting from the static case stabilized in one well, tunneling will lead to an onset of excursions of the ground vibronic state to the two neighboring wells. This quasi-static situation is mirrored by the g-values, which are generalized in the nd^9 case with $(x^2 - y^2)$ type ground state (see figure 1) to

$$g_{\parallel} = g_1 + 2qg_2 \qquad \text{and} \qquad g_{\perp} = g_1 - qg_2. \tag{4}$$

Here q is the 'Ham reduction factor'; it is the ratio between the expectation value of the anisotropic part of the Zeeman operator, calculated with the corresponding vibronic states, as compared to those calculated with the pure electronic parts. For the static case, $q = 1$ (see equation (2)).

It is not only the JT coupling but also the influence of crystal strains which determines the alignment of the E orbitals. If such internal distortions, measured by a quantity δ, representing the average random strain active at the JT site, are stronger than the tunneling splitting 3Γ, $\delta/3\Gamma > 5$, a static situation can result even in the presence of sizable tunneling. Cases falling in the range $0.8 < \delta/3\Gamma < 5$ are termed 'quasi-static' [14]. The competition between tunneling and strain will also influence the EPR lineshapes, usually causing some asymmetry (see figure 2 of [14] or equation (2.5.7) in [11]).

JT coupling and tunneling are internal interactions in a crystal. Therefore, all equivalent axes of JT distortions occur with equal probability and, statistically averaged, the symmetry of a specimen is not lowered with respect to the JT free situation. This is also the case for random internal strains, having no preference direction. The situation changes, if an external uniaxial stress P is applied. Then some of the JT distorted surroundings will be more favorable energetically with respect to the stress direction than other ones. On this basis the application of uniaxial stress will influence both the value of q and the lineshapes, since such stress has the tendency to at least partly impede the tunneling excursions, this influence will thus raise the value of q from its value in the unstressed case towards that of the static one. For this reason the lines will also become more symmetric.

Isotropic lines are expected if all wells contribute equally to the resonances and if the transition rate between the wells $1/\tau \gg \Delta g \mu_B B/h$ (Δg, g-splitting between contributing states; μ_B, Bohr magneton; B, magnetic field). The corresponding states can result from a coherent superposition of the contributions of the three component vibronic orbitals (equation (1)). The states of A-symmetry among these have finite expectation values only of the scalar, isotropic parts of the Zeeman interaction [10, 11]. However, also phonon-induced relaxations between the wells can lead to isotropic resonances. At temperatures high enough that the classical barriers between the three wells are surmounted, motional averaging, corresponding to an equal contribution of all wells, will take place. At lower temperatures, direct and Raman phonon processes can induce reorientation processes between the ground states of the wells, also possibly causing isotropic signals. The linewidths of these isotropic lines, however, show angular dependence, since they arise from averaging between component lines with splittings dependent on the magnetic field orientation. As long as kT is larger than the strain splittings between the ground states of the wells, the transition rate between the wells is independent of the strain size (see [11], equation (2.5.8)). If the converse holds, the strains dominate; then the line positions are not isotropic anymore and eventually the quasi-static appearance of the spectra can result.

The strain induced static, anisotropic signals and the isotropic ones, averaged by one- or more-phonon processes, can be observed simultaneously with the same specimen, if the strains vary throughout the crystal [19]. From regions with low strain sizes isotropic lines can be registered, while those with large strains lead to the anisotropic spectra.

The application of uniaxial stress not only allows us to probe the details of the prevailing influences, which dominate the actual manifestations of the JT effect, but also to determine the strain coupling coefficient V_2. This is based on the fact that externally induced strain is a further agent to lift the degeneracy of the originally degenerate ground state orbitals, as described by the perturbation $H_s = V_2(e_\theta U_\theta + e_\varepsilon U_\varepsilon)$ [10, 11]. Here the strain is represented by $e_\theta = e_{zz} - \frac{1}{2}(e_{xx} + e_{yy})$ and $e_\varepsilon = \frac{1}{2}\sqrt{3}(e_{xx} - e_{yy})$, with strain tensor components $e_{ij} = \frac{1}{2}(\frac{\partial u_i}{\partial x_j} + \frac{\partial u_j}{\partial x_i})$. $U_\theta = \left(\begin{smallmatrix} -1 & 0 \\ 0 & +1 \end{smallmatrix}\right)$ and $U_\varepsilon = \left(\begin{smallmatrix} 0 & +1 \\ +1 & 0 \end{smallmatrix}\right)$ are operators acting on the initially degenerate orbitals. Experimentally, V_2 is derived from the Boltzmann population of the lowest levels resulting from the combined action of JT coupling, internal strains and external stress. Assuming, for simplicity, a discrimination into two JT distorted configurations, an energetically

favorable one, leading to a signal I_{fav} with statistical abundance n_{fav}, and similarly for the unfavorable ones, one finds [20, 21]

$$\ln\left(\frac{I_{\mathrm{fav}}/n_{\mathrm{fav}}}{I_{\mathrm{unfav}}/n_{\mathrm{unfav}}}\right) = \frac{3V_2P}{2kT(c_{11}-c_{12})}. \tag{5}$$

The c_{ii} are components of the stiffness tensor; for the special, approximately cubic case of BT, two of them, c_{11} and c_{12}, are sufficient to characterize the situation [22]. Considering an octahedral cluster with cube length R, reduced mass M and a vibration frequency ω, Ham [10, 11] calculated a relation between V_2 and the JT energy:

$$E_{\mathrm{JT}} = \frac{3V_2^2}{8M\omega^2R^2}. \tag{6}$$

This is derived from a simple model taking only the first neighbors of the JT ion into account.

3. Experimental details

Most of the experiments were performed with a Bruker 200D SRC EPR spectrometer, operating near 9 GHz. Temperatures between 6 and 180 K could be achieved with an Oxford flowing He gas cryostat, regulated with an Oxford ITC instrument. The investigated specimens had typical dimensions of $2 \times 2 \times 3$ mm^3. The treated defects were present as unintended background impurities in nominally undoped crystals. The charge states Ni^+, Pt^{3+} and Fe^{5+} were created from precursor charge states by illumination with the full output of a 150 W xenon arc lamp, while Rh^{2+} was detected without further treatment. The recharging to Ni^+ and Fe^{5+} proceeds by capturing an optically induced conduction band electron by Ni^{2+} and a valence band hole by Fe^{4+}, respectively. The optical creation of such carriers is often observed in oxide perovskites (see, e.g. [1]). The precursor charge state of Pt^{3+} is not known. Uniaxial stress was applied to the crystal using a setup as described by Kool and Lenjer [20, 21]. Due to the geometrical constraints of the EPR equipment only stresses perpendicular to the magnetic field B could be applied.

At temperatures below about 180 K the BT crystals assume the rhombohedral crystal phase, characterized by trigonal, ⟨111⟩-type lattice distortions, resulting from local domains. For the ions Ni^+, Rh^{2+} and Pt^{3+} such low symmetry influences turn out to be so weak that they can be neglected in the present context. The ⟨111⟩ domain fields are not collinear with the ⟨100⟩ JT distortions of all the JT systems studied here. The resulting competition causes slight tilts of the principal axes of the g-tensors of these $S = 1/2$ systems from the ⟨100⟩ directions towards ⟨111⟩. Empirically, it is found that these tilts are rather small, indicating a rather weak influence of the domain field compared to the local JT distortion fields. For the case of Pt^{3+} a corresponding splitting will be shown, see section 4.3. For Fe^{5+} both the off-center excursions and the rhombohedral crystal fields are collinear along ⟨111⟩ directions. Possible influences of the domain fields for this case will be discussed in section 5.

4. Experimental results and their interpretation

4.1. Ni^+ ($3d^9$)

The corresponding EPR signals were first reported by Possenriede *et al* [23] in 1992, but could not be assigned definitely at that time. The angular dependence of the Ni^+ EPR spectra with B rotated in the (001) plane of the crystal at $T = 6$ K is shown in figure 2.

Indicated are the g-values of signals caused by a defect having tetragonal symmetry with axes along ⟨100⟩ type directions. The corresponding g-tensor components are $g_{\parallel} = 2.365$ and

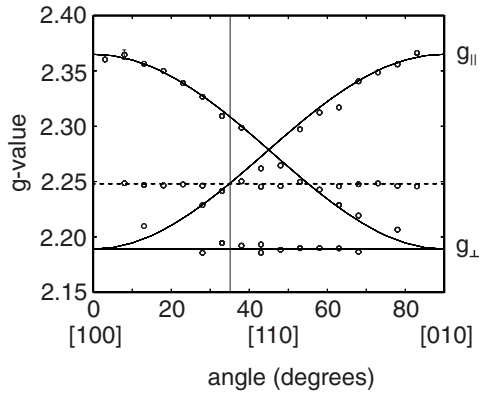

Figure 2. Angular dependence of the Ni^+ resonances, given by the corresponding g-values. Three branches corresponding to a tetragonally distorted environment and one isotropic branch (dashed) are superimposed.

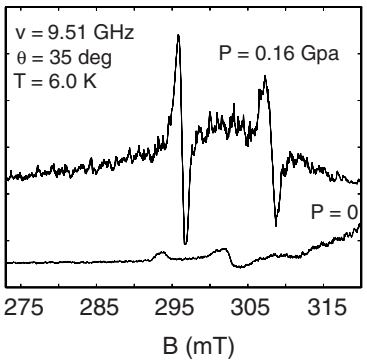

Figure 3. Signals of Ni^+, when B makes an angle of 35° with the [100] direction (vertical line in figures 2 and 4) under $P = 0$ and 0.16 GPa.

$g_\perp = 2.189$. In addition, an isotropic signal with $g_{\rm av} = \frac{1}{3}(g_\parallel + 2g_\perp) = 2.249$ is observed. Its linewidth is strongly angular dependent, being for instance 29 G for $B \parallel [111]$, while it is broadened beyond detection for $B \parallel [100]$ at $T = 6$ K. Furthermore, the shapes of the EPR signals of the tetragonal spectrum are somewhat asymmetric at $P = 0$ (figure 3).

Under application of external uniaxial [001]-stress (note $P \perp B$) the following changes in the EPR spectrum are observed.

(i) The intensity of the two lines stemming from tetragonal centers with their axes perpendicular to the stress direction, i.e. those showing an angular dependence in figure 2, increases; the angular independent one at $g_\perp = 2.189$ decreases; it corresponds to centers with their axes parallel to the stress direction. The latter line cannot be observed at stresses higher than 0.16 GPa, when all intensity has been transferred to the angular dependent ones. Under stress the observable lines become more symmetric. These facts are visualized in figure 3, exhibiting the EPR spectrum at stresses $P = 0$ and 0.16 GPa and at $T = 6.0$ K. Figure 4 shows the angular dependence of the Ni^+ spectra for B rotated in the (001) plane of the crystal under an externally applied uniaxial [001] stress of $P = 0.20$ GPa.

(ii) The $g_\perp$-value becomes smaller under increasing uniaxial stress, whereas $g_\parallel$ remains unchanged. The difference $\Delta g = g_\parallel - g_\perp$ thus increases.

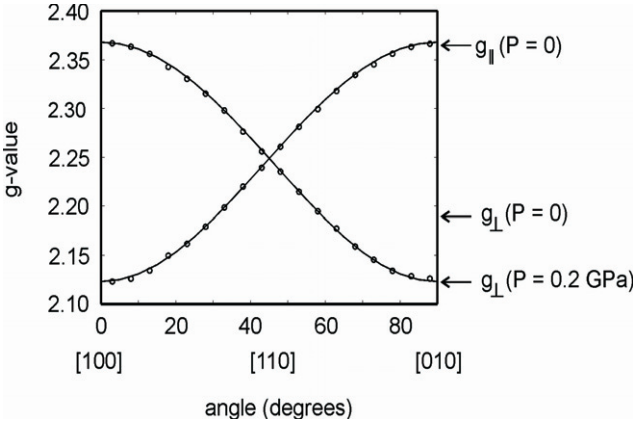

Figure 4. Angular dependence of line positions of Ni^+ under uniaxial stress along a 100-type direction.

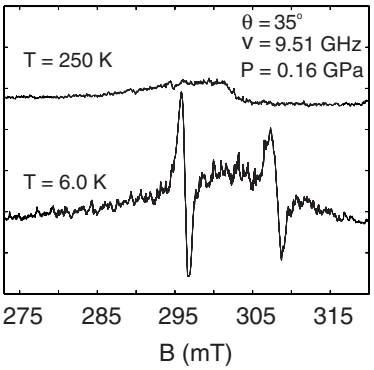

Figure 5. Turnover from an anisotropic spectrum of Ni^+ at low temperatures to an isotropic one at elevated temperatures.

(iii) Under rising temperatures first a line broadening occurs and at higher temperatures a transition from an anisotropic to an isotropic spectrum is observed (figure 5).

No hyperfine lines are detected. This does not contradict the assignment to Ni^+, to be detailed below, because the only Ni isotope with nonzero nuclear spin, ^{61}Ni, having $I = 3/2$, has a natural abundance of only 1.13%. Each of the expected four hyperfine lines thus has only an intensity of 0.3% relative to the central $I = 0$ line. Under the prevailing signal to noise conditions they cannot be detected.

The relative weights of the isotropic and the anisotropic signals depend strongly on the thermal history of the samples and the application of uniaxial stress. This is illustrated by the following representative observations.

(i) If a stress $P = 0.2$ GPa is applied at 6 K, the isotropic line at $g = 2.249$ (dashed in figure 2) disappears and the intensity of the tetragonal spectrum increases.

(ii) In an experiment where the specimen was cooled quickly to 4.2 K by adding liquid helium to a cryostat holding the crystal, only the isotropic line was observed, at $g = 2.248$.

(iii) If, under this experimental condition, a uniaxial stress $P = 0.048$ GPa is applied, the isotropic line shifts from $g = 2.248$ to 2.255 and two anisotropic lines appear, characterized by

$g_\parallel = 2.364$ and $g_\perp = 2.139$. Their widths are, respectively, 12 and 31 G. These findings are in line with those of the previous experiments.

We shall now interpret the experimental observations. First the assignment to Ni^+ ($3d^9$) will be proved and then the JT related features of the system will be pointed out. The observed values of the g-tensor components are typical for Ni^+, but could possibly also be assigned to strong field Ni^{3+} [24]. The alignment under stress, however, is compatible only with Ni^+. First, the observation that $g_\parallel > g_\perp$ indicates that an $(x^2 - y^2)$ type orbital is the ground state (equation (1)). Since the application of stress increases the concentration of centers with axes perpendicular to the stress direction, they are characterized by spontaneously elongated octahedra (figure 1). For an elongated octahedron a $(x^2 - y^2)$ orbital ground state occurs only for a hole state. This establishes Ni^+ ($3d^9$) as the charge state of the investigated defect. For the alternative case (Ni^{3+} ($3d^7$)), only the strong field case could show g-values in the range of the observed ones [24]. But then $g_\parallel < g_\perp$ should be found for the identified situation of an elongated octahedron, see below, where cases of this type, i.e. Rh^{2+} and Pt^{3+}, are treated. The assignment to Ni^+ is further supported by the recent identification of the defect Ni^+_{Ba} in BT [25], i.e. of Ni^+ found at a Ba site where it goes off-center, as also identified by the application of uniaxial stress. The average g-value of this defect, 2.25, is identical within experimental error to that treated here. This comparison with Ni^+_{Ba}, having otherwise slightly different g-tensor components, supports the assignment of the present defect to Ni^+ replacing Ti^{4+}, implicitly assumed so far.

The application of uniaxial stress first proves that a JT effect is active: the alignment of the tetragonal defect axes occurs as fast as the EPR spectra can be observed, i.e. within a few seconds; this takes place even at low temperatures (4.2 K) and low stresses. If the tetragonality were caused by association of an ionic defect, the reorientation would be very slow or practically forbidden at low temperatures. Also, the fact that a motionally averaged spectrum is observed for $T > 46$ K argues for the presence of a JT effect.

The tetragonality of the defects then indicates that the JT distortion is caused by coupling of the E-orbital ground state to an e-vibration distortion (figure 1). The question arises of whether the axes are strictly aligned, as characteristic for a static JT effect, or whether there are still excursions to neighboring wells, due to an onset of tunneling. Application of uniaxial stress will reduce such excursions and thus increase the axiality. Exactly this is observed: the g-tensor anisotropy increases under stress. Therefore, the unstressed case rather corresponds to a 'quasi-static' situation. Quantitatively, this is expressed by an increase of the reduction factor q towards unity. For the quasi-static situation the g-values are expressed by $g_\parallel = g_1 + qg_2$ and $g_\perp = g_1 - 2qg_2$ (equation (4)). At the highest stresses tolerated by the given crystal specimens we obtain $qg_2 = \frac{1}{3}(g_\parallel - g_\perp) = 0.082$ and $g_1 = g_\parallel - qg_2 = 2.282$. In the similar case of Ni^+ in MgO the values $qg_2 = 0.145$ and $g_1 = 2.2391$ [19] were found. Apparently in our case q is not as large as for MgO. Therefore BT:Ni^+_{Ti} is not completely in the 'pure' static region, even at the maximal stress. This is also confirmed by the observation that the two remaining EPR lines still have somewhat different widths (figure 5).

The line shapes become more symmetric under stress: this is in line with the fact that uniaxial stress represses the state mixing by tunneling, as outlined in section 3.

Among the isotropic lines, two types are observed: one arises at elevated temperatures, $T \sim 25$ K, certainly due to a motional averaging by jumping across the classical barriers, from the signals reflecting the static JT effect. The other type of such signals is found at low temperatures simultaneously with the tetragonal ones. These features point to a phonon-assisted relaxation process between the ground states of the wells. Apparently, in some regions of the investigated specimens the sizes of the strains are low enough that kT is larger than the strain splittings between the wells. As mentioned in section 3, then the influence of strains on

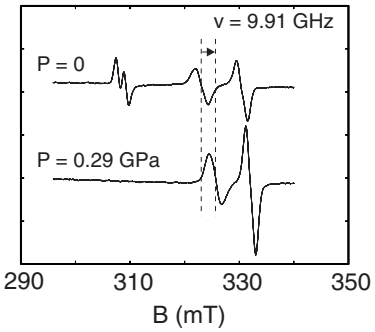

Figure 6. EPR spectra of Rh^{2+}, for B at 40° from [100] in the (001) plane, without and under uniaxial stress at $T = 5.0$ K; see figure 7. The low field signal, with $B \perp z$, characterized by a Rh hyperfine splitting into two lines, vanishes with rising stress and the other signals increase correspondingly. For these the Rh hyperfine splitting is too small to be resolved. The arrow indicates the change of a line position under uniaxial stress.

the isotropic lines is reflected at most in the angular variation of the linewidths. Spectra related to tetragonally stabilized centers originate from regions of higher strains. This simultaneous presence of two types of signals has also been reported previously for Ni^+ in MgO [19].

The changes of the relative intensities of anisotropic and isotropic lines under slight external influences (uniaxial stress or temperature changes) indicate the fragility of the undistorted low strain order of BT: for instance, it is seen that under application of uniaxial stress the isotropic line may vanish completely, indicating the increasing disorder introduced in this way. On the other hand, in one experiment it appeared that fast cooling to liquid helium temperature established a situation with low strains throughout the sample. Furthermore, slight variations of the g-tensor components, in some instances observed under the specified treatments, point to the influence of tunneling, depending on local order, on these spectral parameters.

Unfortunately, the strain coupling coefficient of Ni^+ could not be determined because the related EPR signals interfered on their high field side, i.e. near the position of the isotropic signal in figure 2, with those originating from Fe^{3+}.

4.2. Rh^{2+} ($4d^7$)

This defect is characterized [23] by an electronic spin $S = 1/2$, a hyperfine coupling to a 100% abundant nuclear spin $I = 1/2$ (as for ^{103}Rh), a tetragonal g-tensor with components $g_\parallel = 2.030$ and $g_\perp = 2.298$ and a turnover of the corresponding angular dependent lines to a motionally averaged, isotropic one for $T > 46$ K. All these features support the assignment to an E ⊗ e JT effect. Here we present new details on the JT coupling, obtained by application of uniaxial stress along [001]. The following changes in the EPR spectra were observed:

(i) As in the previous case of Ni^+, the intensity of the signals stemming from tetragonal centers with their axes perpendicular to the stress direction increases and the concentration of axes parallel to the stress direction decreases. The latter lines are not observable anymore at stresses higher than 0.25 GPa (figure 6).

(ii) The $g_\perp$-value decreases (see figure 7), and since $g_\parallel$ is not changed by stress, the difference $\Delta g = g_\parallel - g_\perp$ becomes smaller. Figure 7 shows the angular dependence of the EPR spectrum with B rotated in the (001) plane (perpendicular to P) of the crystal ($P = 0.24$ GPa).

From the observed intensity changes (figure 8) of the EPR signals the strain-coupling coefficient V_2 could be determined.

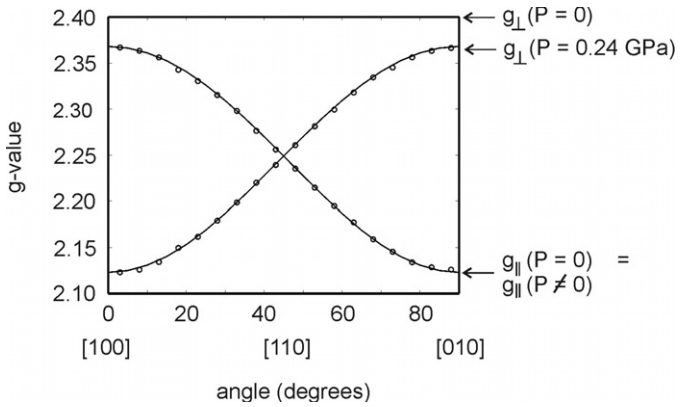

Figure 7. Angular dependence of the EPR signals of Rh^{2+} under a uniaxial stress of 0.24 GPa.

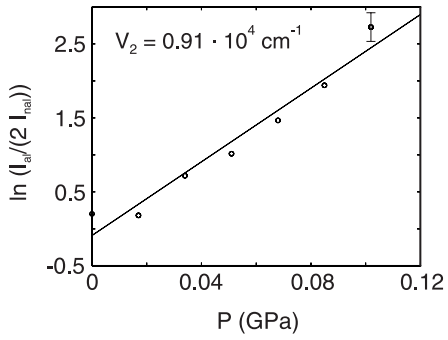

Figure 8. Occupation ratio of aligned and not aligned defect axes, in logarithmic scale, versus the strength of the applied uniaxial stress.

The fast reorientation of the tetragonal defect axes and the transition to a motionally averaged, isotropic spectrum at elevated temperatures again proves that an E ⊗ e JT effect is active. In the same way as for Ni^+, it is also concluded that an elongated octahedron is present: the axes align perpendicular to the stress direction. In the present situation, however, the fact that $g_\parallel < g_\perp$ indicates that a $3z^2 - r^2$ orbital lies lowest. This is consistent with a single unpaired electron. The interpretation of figure 8, using equation (5), leads to the stress coupling coefficient $V_2 = 0.91 \times 10^4$ cm^{-1}. Interpreting this quantity on the basis of the simple cluster model (equation (6)) yields a JT energy $E_{JT} = 404$ cm^{-1}, if a representative phonon energy of 200 cm^{-1} is assumed [11]. This is a rather low value for E_{JT}, if compared, e.g. to $E_{JT} = 3000$ cm^{-1} for Al_2O_3:Ni^+ [11]. For a small JT energy a dynamic JTE would be expected, characterized by two lines. The fact that, in spite of this, spectra of a tetragonally distorted center are observed indicates that considerable internal strains are active, stabilizing the tetragonal distortions. The g-anisotropy becomes smaller under stress (figure 7), indicating that the crystal field splittings increase.

4.3. Pt^{3+} ($5d^7$)

The Pt^{3+} center in BT [23, 26–28] has the following properties: $S = 1/2$, hyperfine interaction typical for ^{195}Pt (34% $I = 1/2$), approximate tetragonality with $g_\parallel = 1.958$, $g_\perp = 2.455$.

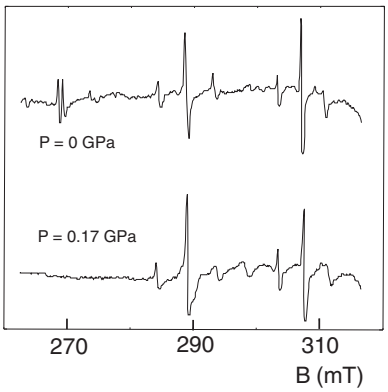

Figure 9. Spectra of Pt^{3+} at 4.2 K for B 35° away from [100] in the (001) plane, under $P = 0$ GPa (above) and $P = 0.17$ GPa (below). Compare with the stress dependence of the Rh^{2+} spectra (figure 6). The weak splitting of the low field line for $P = 0$ GPa, best seen for the $I = 0$ isotopes, is caused by the competition between the ⟨111⟩ rhombohedral domain fields and the ⟨100⟩ local JT distortions [23].

Several observations support the assignment to an E ⊗ e JT effect. This model can account in particular for the unusual angular dependence of the intensities of the hyperfine lines of ^{195}Pt, when compared with those of the remaining nuclei, having $I = 0$. These features consist in a pronounced different saturation behavior of these lines, when compared to the $I = 1/2$ signals [23]. The phenomena are successfully explained by a hyperfine induced electron spin relaxation having an angular dependence typical for an E ⊗ e JT effect [11]. Also the motional averaging of the spectra at elevated temperatures, $T > 100$ K [29], supports an interpretation in terms of an E ⊗ e JT effect.

The application of uniaxial [001] stress yields the following results, quite similar to those observed for Rh^{2+}.

(i) As in the previous cases, the intensity of the lines resulting from tetragonal centers with their axes perpendicular to the stress direction increases and the intensity of that parallel to P decreases; the corresponding line is not observable anymore at stresses higher than 0.16 GPa (figure 9).

(ii) The value of $g_\perp$ decreases: $g_\perp = 2.455$ at zero stress and $g_\perp = 2.452$ at $P = 0.17$ GPa. There is no observable shift of the $g_\parallel$ value under the influence of stress, so Δg becomes smaller.

(iii) The hyperfine coupling value $A_\perp$ increases from $A_\perp = 111 \times 10^{-4}$ cm^{-1} at zero stress to 115×10^{-4} cm^{-1} at $P = 0.17$ GPa. The $A_\parallel$ value hardly changes under increasing stress, so $\Delta A = A_\parallel - A_\perp$ becomes larger. In listing these $g_\perp$ as well as the $A_\perp$ values we did not consider small deviations stemming from the rhombohedral phase of BT.

As in the previous cases, the center aligns with its axis perpendicular to the stress direction; thus the octahedron surrounding Pt^{3+} is elongated. Just as for Rh^{2+} the strain coupling coefficient could be determined: $V_2 = 0.60 \times 10^4$ cm^{-1}; this value is of a size comparable to that of Rh^{2+} and differs considerably from that claimed previously [26] for Pt^{3+}, $V_2 = 2.87 \times 10^4$ cm^{-1}. The now established smaller value of V_2 corresponds to $E_{JT} = 180$ cm^{-1} (equation (6)). The tetragonality, observed in spite of this small stabilization energy, again points to a strong influence of internal strains. Also, the decrease of Δg under stress can be attributed to the fact that stress decreases the deviations from strict alignment.

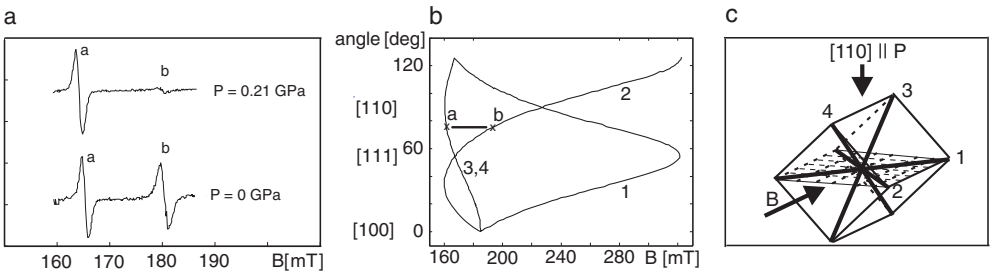

Figure 10. (a) EPR signals of Fe^{5+} in $BaTiO_3$ under $P = 0$ and 0.21 GPa. The letters refer to the branches of the angular dependence plot in (b). (b) Angular dependence of the Fe^{5+} EPR signals for a rotation of B in a (110) plane, as indicated in (c). Each of the branches corresponds to one of the four equivalent centers, axially symmetric around the body diagonals, numbered in (c). This means that EPR line a is caused by centers with axes along body diagonals 3 and 4, line b correspondingly by 1 and 2. (c) The correlation between the body diagonals of a BT crystal, the numbers of the branches in (b) and the direction of the stress axis.

5. Off-center Fe^{5+}

The EPR of Fe^{5+} in BT (see figure 10) is described [30] by a Hamiltonian:

$$H^{\text{eff}} = \mu_{\text{B}} \boldsymbol{S}^{\text{eff}} \boldsymbol{g}^{\text{eff}} \boldsymbol{B} \tag{7}$$

(μ_{B} Bohr magneton) with an effective spin $S^{\text{eff}} = 1/2$ and a g-tensor with essentially $\langle 111 \rangle$-type axial symmetry, having the following components: $g_{\parallel}^{\text{eff}} = 2.010(3)$; $g_{\perp}^{\text{eff}} = 4.013(3)$. In fact, resonances resulting from a superposition of four such axial centers are observed, with axes defined by the four body diagonals (figure 10(c)). These numerical values are typical for a system with a true spin $S = 3/2$ and an orbitally non-degenerate ground state, as expected for a $(3d)^3$ ion in octahedral symmetry, which is additionally exposed to a strong axial crystal field component. For the actual spin $S = 3/2$ the appropriate, axially symmetric Hamiltonian is

$$H = \mu_{\text{B}} \boldsymbol{S} \boldsymbol{g} \boldsymbol{B} + D(S_z^2 - \tfrac{1}{3} S(S+1)). \tag{8}$$

If the splitting $|2D|$ between the $|m_S| = |1/2\rangle$ and $|m_S| = |3/2\rangle$ substates is much larger than the used microwave quanta ($\sim$0.3 cm^{-1} in the present case), it is allowed to truncate the $S = 3/2$ spin space to the $|m_{\text{s}}| = |1/2\rangle$ subspace of the lower lying doublet, spanned by an effective spin $S^{\text{eff}} = 1/2$. The Zeeman splitting is then described by the effective Hamiltonian (equation (7)). The components of the effective g-tensor g^{eff} are related to the 'true' g-values, $g_{\parallel}$ and $g_{\perp}$, by the perturbative expression [35]

$$g_{\perp}^{\text{eff}} = 2g_{\perp}\left\{1 - \frac{3}{4}\left[\frac{g_{\perp}\mu_{\text{B}}B}{2D}\right]^2\right\}, \qquad g_{\parallel}^{\text{eff}} = g_{\parallel}. \tag{9}$$

The values $g_{\parallel} = 2.010(3)$ and $g_{\perp} = 2.013(3)$ are found. Here it is surprising that these are larger than the g-value for the free spin, $g_{\text{s}} = 2.002$. For nd-shells less than half filled, as for Fe^{5+}, one expects g-values smaller than g_{s}. In their study of the $3d^3$ ions Cr^{3+}, Mn^{4+} and Fe^{5+} in $SrTiO_3$ (ST), Müller *et al* [32, 33] have shown that this discrepancy has to be attributed to the admixture of valence band O^- hole states to the Fe^{5+} ground state, having levels close to the valence band edge. Equation (9) allows us to determine the value of D from measurements at two different values of B, corresponding to two different microwave frequencies. For Fe^{5+} in BT $|D| = 1.15\ \text{cm}^{-1}$ is found [30], to be compared with $|D| = 0.65\ \text{cm}^{-1}$ for the isoelectronic

ions Mn^{4+} [31] and $|D| = 0.023\ cm^{-1}$ for Cr^{3+} [34] in BT. All these values are valid for $T = 20$ K and below. This sequence of D values leads to the supposition that Fe^{5+} sits especially strongly 'off-center', as supported by its small ionic radius.

The application of uniaxial stress P leads to the following phenomena: with increasing stress and P perpendicular to B, with B lying in the (110) plane and rotated a few degrees from the [111] direction towards the [110] axes of the crystal (see figure 10), it is observed that the low field line (a in figure 10) increases in intensity at the cost of the high field line, b. Figure 10 shows the effect of applying uniaxial stress up to $P = 0.21$ GPa. At $P = 0.23$ GPa the high field line is not observable anymore.

Figure 10(c) demonstrates the orientation of the stress axis with respect to the ⟨111⟩-type body diagonals of the crystal. The diagonals 1 and 2, lying in a (110) plane, are directed perpendicular to the stress axis, while diagonals 3 and 4 have components parallel to it. Since resonance a, corresponding to branches 3 and 4, increases with rising stress, while that of b decreases, it is seen that the axes of the center reorient, with the ⟨111⟩ directions parallel to the stress axis being favored. This means that the oxygen octahedron surrounding Fe^{5+} adapts to its presence by a trigonal axial compression. This oblate, lens-like geometry favors orientation of the axis parallel to the stress direction. Since the reorientation occurs at low temperatures ($T = 30$ K) as fast as the EPR signals can be observed (a few seconds), this observation clearly shows that the trigonal symmetry is an intrinsic property of the Fe^{5+}–O_6 cluster and not caused by the possible association with a second ionic defect.

The rearrangement is not caused by a JT effect, since the ground state of Fe^{5+} is orbitally non-degenerate. An Fe^{5+} defect, going off-center from its Ti^{4+} home site along one of the ⟨111⟩-type body diagonals, is the natural explanation for the stress dependence. This is supported by the following observations: Cr^{3+}, charged negatively with respect to Ti^{4+}, is repelled by its negative O^{2-} ligands [31] and thus shows a rather low trigonal crystal field parameter. Mn^{4+} participates in the same ferroelectric off-center excursions as the Ti^{4+} ions [31]. The positive charge and low ionic radius of Fe^{5+} support a further movement towards one of the neighboring triangles of three O^{2-} ions along a body diagonal of the oxygen cube. This situation corresponds to a trigonally compressed octahedron.

The stress dependence of the alignment ratio (figure 11) allows us to quantify the coupling of the defect to the lattice. At zero stress, the low field line a (branches 3 and 4 in figure 10) should have twice the intensity of the high field line, b, branch 2. In plotting $\ln(I_a/2I_b)$ versus the stress $P_{[011]}$ (figure 11) and assuming a Boltzmann distribution, the elastic dipole moment $\beta_{[111]}$ could be determined from $\ln(I_a/2I_b) = \Delta U/kT$ with $\Delta U = \beta_{[111]}P_{[011]}$. Deviations from linearity at low P are caused by an unequal initial presence of the four ⟨111⟩ off-center excursions. It can be assumed that the off-center movements are biased by the local domain fields or by local strains. In the first case the measured ratio $(I_a/2I_b)$ would mirror the relative weights of the domains present in the investigated specimen. Since, however, for the JT ions Ni^{+}, Rh^{2+} and Pt^{3+} it was observed (section 3) that the influence of the domain fields was weak compared to the fields caused by the local JT distortions, the same is likely to occur also for the fields originating from the local off-center excursions. The transition to the linear part of the graph (figure 11) would then take place, if the action of external strain overrides the influence of local strains. A final decision concerning the role of the domain fields cannot be made in the present case of Fe^{5+} in BT nor in the parallel case of Mn^{4+} [34], where the action of external strain was not investigated.

From the linear part of the graph in figure 11 the value $\beta_{[111]} = 4.13 \times 10^{-30}\ m^3$ is determined (for information on the physical background of β, see [35]). This value is of the same size as those found for the Ni^{+}_{Ba} and Na^{+}–O^{-} centers [25, 36] in BT and the systems Fe^{2+}–O^{-} and Cr^{5+} in ST [35, 37].

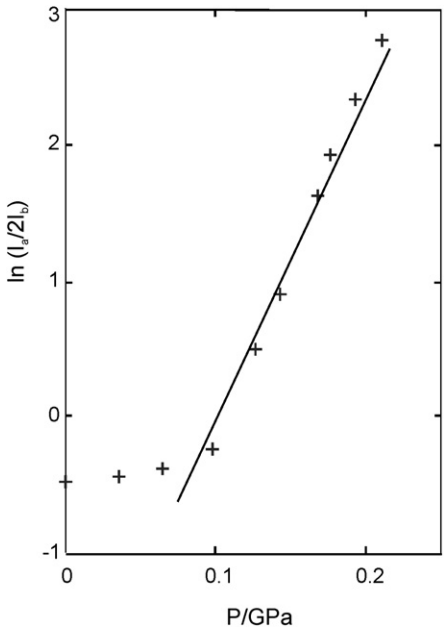

Figure 11. Stress dependence of the signal ratio of favorable versus unfavorable off-center orientations in BT:Fe^{5+}.

The question arises of why Fe^{5+} in BT behaves so differently to Fe^{5+} in ST. In the latter case an isotropic signal is observed [32], independent of temperature, and all features indicate that the small Fe^{5+} ion tunnels fast between several equivalent off-center positions [32]. Judging from the behavior of Cr^{5+} in $SrTiO_3$, which goes off-center along ⟨100⟩-type tetragonal directions in this material [38], an analogous situation would be expected for Fe^{5+}. Its off-center displacement in BT along ⟨111⟩ could be caused by the slightly larger lattice constant of BT, 4 Å, about 2% more than that of ST. In the latter system Fe^{5+} thus tends to be pushed back on-site, whereas it has more space to move off-center in BT, in the same way as the Ti^{4+} host ions of this ferroelectric material.

6. Conclusion

Three ions, Ni^{+}, Rh^{2+} and Pt^{3+}, have been identified to show an E ⊗ e JT effect in BT. The application of uniaxial stress definitely led to the conclusion that a related spontaneous symmetry lowering and not an association with an ionic defect is present, which is a possible reason for the observed low defect symmetries. Furthermore, uniaxial stress allowed us to determine in two cases the stress coupling of the defects and to give an estimate of the related JT energies. They turned out to be rather low, which led to the conclusion that the observed phenomena, consistent with static JT effects, were mainly due to a stabilization of the JT effects by internal strains. Some observations allowed the conclusion that the influence of tunneling between the equivalent distortions is playing a role. On this basis the changes of g-values and lineshapes induced by the application of uniaxial stress could be explained. The stress response of Fe^{5+} in BT, in contrast, is caused by the off-center movement of this ion. It constitutes a further manifestation of iron contaminations in BT as well as in other oxide perovskites, causing their coloration [39] in the 'as-grown' state in spite of their large band gaps.

References

[1] Briat B, Grachev V G, Malovichko G I, Schirmer O F and Woehlecke M 2006 Defects in inorganic photorefractive materials and their investigations *Photorefractive Materials and Their Applications* vol 2, ed P Guenter and J P Huignard (Berlin: Springer) pp 9–49
[2] Langhammer H T, Müller T, Böttcher R and Abicht H P 2003 *Solid State Sci.* **5** 965
[3] Dunbar T P, Warren W L, Tuttle B A, Randall C A and Tsur Y 2004 *J. Phys. Chem.* B **108** 908
[4] Lenjer S, Schirmer O F, Hesse H and Kool Th W 2002 *Phys. Rev.* B **66** 165106
[5] Kolodiazhnyi T and Wimbush S C 2006 *Phys. Rev. Lett.* **96** 246404
[6] Schirmer O F 2006 *J. Phys.: Condens. Matter* **18** R667
[7] Lenjer S, Schirmer O F, Hesse H and Kool Th W 2004 *Phys. Rev.* B **70** 157102
[8] Jahn H A and Teller E 1937 *Proc. R. Soc.* A **161** 220
[9] Abragam A and Bleaney B 1970 *Electron Paramagnetic Resonance of Transition Metal Ions* (Oxford: Clarendon)
[10] Ham F S 1968 *Phys. Rev.* **166** 307
[11] Ham F S 1972 *Electron Paramagnetic Resonance* ed S Geschwind (New York: Plenum)
[12] Boatner L A, Reynolds R W, Abrahams M M and Chen Y 1973 *Phys. Rev. Lett.* **31** 7
[13] Reynolds R W, Boatner L A, Abrahams M M and Chen Y 1974 *Phys. Rev.* B **10** 3802
[14] Reynolds R W and Boatner L A 1975 *Phys. Rev.* B **12** 4735
[15] Setser G G, Barksdale A O and Estle T L 1975 *Phys. Rev.* B **12** 4720
[16] Bersuker J B 2006 *The Jahn–Teller Effect* (Cambridge: Cambridge University Press)
[17] Raizman A, Suss J T and Low W 1977 *Phys. Rev.* B **15** 5184
[18] Raizman A, Schoenberg A and Suss J T 1979 *Phys. Rev.* B **20** 1863
[19] Schoenberg A, Suss J T, Luz Z and Low W 1974 *Phys. Rev.* B **9** 2047
[20] Kool Th W 1991 *PhD Thesis* University of Amsterdam
[21] Lenjer S 1999 *PhD Thesis* University of Osnabrück
[22] Landolt H and Börnstein R 1992 *Numerical Data and Functional Relationships in Science and Technology* (*New Series* III 29a) (Berlin: Springer)
[23] Possenriede E, Jacobs P and Schirmer O F 1992 *J. Phys.: Condens. Matter* **4** 4719
[24] Müller K A, Berlinger W and Rubins R S 1969 *Phys. Rev.* **186** 361
[25] Lenjer S, Scharfschwerdt R, Kool Th W and Schirmer O F 2000 *Solid State Commun.* **116** 133
[26] Bukhan'ko F N and Bratashevskii Y A 1981 *Sov. Phys.—Solid State* **23** 456
[27] Sroubek Z, Zdansky K and Simanek E 1963 *Phys. Status Solidi* **3** K1
[28] Simanek E, Sroubek Z, Zdansky K, Kaczer J and Novak L 1966 *Phys. Status Solidi* **14** 333
[29] Bukhan'ko F N 1980 *Sov. Phys.—Solid State* **22** 1174
[30] Possenriede E, Schirmer O F, Donnerberg H J, Godefroy G and Maillard A 1998 *Ferroelectrics* **92** 245
[31] Müller K A, Berlinger W, Blazey K and Albers J 1987 *Solid State Commun.* **61** 21
[32] Müller K A, von Waldkirch Th, Berlinger W and Faughnan B W 1971 *Solid State Commun.* **9** 1097
[33] Schirmer O F, Berlinger W and Müller K A 1975 *Solid State Commun.* **16** 1289
[34] Müller K A, Berlinger W and Albers J 1985 *Phys. Rev.* B **32** 5837
[35] Kool Th W and Glasbeek M 1993 *J. Phys.: Condens. Matter* **5** 361
[36] Varnhorst T, Schirmer O F, Kröse H, Scharfschwerdt R and Kool Th W 1996 *Phys. Rev.* B **53** 116
[37] Kool Th W, de Jong H J and Glasbeek M 1994 *J. Phys.: Condens. Matter* **6** 1571
[38] Müller K A, Blazey K W and Kool Th W 1993 *Solid State Commun.* **85** 381
[39] Meyer M, Schirmer O F and Pankrath R 2004 *Appl. Phys.* B **79** 395